ANNUAL REVIEWS

Annual Review of Materials Research

Cold Sintering: Progress, Challenges, and Future Opportunities

Jing Guo, Richard Floyd, Sarah Lowum, Jon-Paul Maria, Thomas Herisson de Beauvoir, Joo-Hwan Seo, and Clive A. Randall

Materials Research Institute and Department of Materials Science & Engineering, The Pennsylvania State University, University Park, Pennsylvania 16802, USA; email: car4@psu.edu

Annu. Rev. Mater. Res. 2019. 49:275–95

The *Annual Review of Materials Research* is online at matsci.annualreviews.org

https://doi.org/10.1146/annurev-matsci-070218-010041

Keywords

low-temperature sintering, cold sintering, sintering mechanism, ceramics, composites

Abstract

Cold sintering is an unusually low-temperature process that uses a transient transport phase, which is most often liquid, and an applied uniaxial force to assist in densification of a powder compact. By using this approach, many ceramic powders can be transformed to high-density monoliths at temperatures far below the melting point. In this article, we present a summary of cold sintering accomplishments and the current working models that describe the operative mechanisms in the context of other strategies for low-temperature ceramic densification. Current observations in several systems suggest a multiple-stage densification process that bears similarity to models that describe liquid phase sintering. We find that grain growth trends are consistent with classical behavior, but with activation energy values that are lower than observed for thermally driven processes. Densification behavior in these low-temperature systems is rich, and there is much to be investigated regarding mass transport within and across the liquid-solid interfaces that populate these ceramics during densification. Irrespective of mechanisms, these low temperatures create a new opportunity spectrum to design grain boundaries and create new types of nanocomposites among material combinations that previously had incompatible processing windows. Future directions are discussed in terms of both the fundamental science and engineering of cold sintering.

1. INTRODUCTION

Sintering powdered materials into dense, strong, monolithic bodies is an ancient manufacturing method that relies traditionally on high temperatures and long times (1). Some of the earliest identified human-made materials were sintered clay-based ceramics, such as the Venus of Dolní Věstonice, that originated from the upper Paleolithic era approximately 25,000 years ago (2). For millennia, ceramic science progressed along a steady path of continuous refinement, and during this time, great sophistication evolved in formulation engineering, purification, forming, and firing (3). Conventional ceramics are categorized into multiple families, including earthenware, stoneware, porcelain, and bone china. Ceramic production initially developed to address fundamental technology needs such as water vessels and cooking utensils and then transitioned to decorative tiles, sculptures, artware, and tableware worldwide. Industrial ceramics emerged to support high-temperature manufacturing and infrastructure applications that required refractories, bricks, electrical insulation, and crucibles that could survive more extreme environments with much greater purity and microstructure control. These developments initiated the ceramic engineering industrial discipline and a formalized ceramic science education and research enterprise within colleges, universities, and institutes. A common thread linking the efforts of antiquity and modernity is the need for heat treatments that convert a particulate compact to a dense polycrystal.

Theoretical models from Frenkel, Coble, Kingery, and others emerged in the mid-twentieth century and established the foundations of modern sintering science (4–7). The spectrum of sintering techniques expanded during the last 50 years to include a number of alternative approaches that are summarized in **Table 1**. Methods of particular interest include hot pressing (HP), microwave sintering, spark plasma sintering (SPS), flash sintering, and hydrothermal sintering. These are presented in the context of their respective pros and cons, with several examples of typical materials well suited for each technique. References are given to provide the interested readers with details of these techniques. To establish a background against which to compare cold sintering, a brief summary is also provided for each technique.

1.1. Hot Pressing

HP involves the application of pressure during heating in a forming die. In most cases, this pressure is uniaxial, but it remains possible to apply isostatic pressure, as in hot isostatic pressing (HIP). However, HIP is mainly used as a postsintering treatment dedicated to removing final porosity and to obtaining transparent ceramics (8). In comparison to free sintering, HP offers a reduced temperature profile. HP densification is driven by three mechanisms: plastic flow, grain rearrangement (grain sliding), and stress-enhanced diffusion (9). Because plastic flow is a predominant high-temperature mechanism in metals and alloys, HP finds great interest in powder metallurgy and substantially less in ceramics. It is frequently used in the case of ultrahigh-temperature ceramics, such as TiB_2, ZrB_2, SiC, and ZrC (10–12), and some dielectric materials with slow sintering kinetics, such as $(K,Na)NbO_3$ (13).

1.2. Microwave Sintering

Microwave heating enables high thermal ramp rates, a substantial reduction of sintering time, high-purity and high-temperature conditions, fine microstructures via selective and volumetric heating, and in many cases improved mechanical properties (14–17). Due to contrast in the high-frequency dielectric function, many materials react differently for the same incoming energy. In well-controlled instruments with uniform field distributions, microwave sintering offers the advantage of uniform heating because the sample itself is the susceptor, and thermal conductivity

Table 1 Comparisons of alternative sintering techniques

Technique	Pros	Cons	Material examples	References
Hot pressing	High densities Limited grain growth	Batch process	$Pb(Zr,Ti)O_3$ $(Ba,Sr)TiO_3$ Diamond	36, 37
Microwave sintering	Lower temperatures Faster process Multimode or single mode High densities	Limited success in mass production Inhomogeneity in coupling Limited yields for large parts	Al_2O_3 BN $BaTiO_3$ WC Metals	14–17, 38, 39
Spark plasma sintering	Wide range of materials Enhanced densification	Batch process Upscaling High cost	Metals $BaTiO_3$ ZrO_2 SiC AlN	19, 40–43
Flash sintering	Densified, very fast rates Limited grain growth	Microcracking in thermal shocking	ZrO_2 $SrTiO_3$	23, 44
Hydrothermal sintering	Low temperatures Environmentally friendly Metastable materials can be sintered	Long processing times Lower densities in some cases	TiO_2 SiO_2 (amorphous and quartz) ZrO_2 $BaTiO_3$	29, 30, 45–47
Fast firing	Fast process Scalable, continuous manufacturing with roller kilns Limited grain growth Controlled interfaces Atmosphere control	High temperatures High residual stress with cofiring	$BaTiO_3$ Tiles ZrO_2 Al_2O_3	32, 34, 48

requirements are modest. Heating can be very rapid, depending on the material, the insulation, and furnace design.

Ceramics with unique combinations of microstructure and heat treatment can be prepared by microwave sintering, for example (14), fine-grained Al_2O_3 with 98% density, sintered at only 1,400°C with no hold time (15). The same density is obtained under conventional sintering for a treatment of 2 h at 1,600°C with substantial grain growth. Reduced thermal budgets provide access to fully densified materials with well-controlled nanostructure.

However, microwave sintering is usually used at high temperatures (>800°C) and is restricted to ceramics with dielectric functions that provide substantial microwave absorption at some temperature range. Materials with low microwave coupling typically become absorptive at elevated temperatures; in these cases, susceptors located in the periphery of the green bodies can provide the initial heating (16).

1.3. Field-Assisted Sintering Techniques: Spark Plasma Sintering

Field-assisted sintering techniques (FAST) are important because they can produce dense ceramics in time intervals as short as a few seconds for many different ceramic formulations. While local temperatures are difficult to quantify, macroscopically, field-assisted sintering temperatures appear to be lower relative to conventional processes (18). Moreover, SPS is not restricted to metals and ceramics; polymer materials can be densified as well (19). The primary drawback of this technique

is system complexity, resulting in substantial instrumentation expense and less obvious pathways for scale-up to industrial production.

The rapid ramp rates and low macroscopic temperatures accessed in FAST methods create important new processing opportunities. For example, SPS was recently used to densify ZnO, with the addition of water, at 250°C (20). Moreover, with the addition of pressure, SPS can be used to stabilize and densify materials with limited thermodynamic stability (i.e., phases subject to structural transitions or decomposition events during the firing schedule that eliminate the possibility of a conventional approach) (21, 22).

A related field-assisted technique is flash sintering. Perhaps its most remarkable asset is the highly improved sintering kinetics, with full densification of refractory ceramics, such as YSZ or Al_2O_3, obtained in seconds (23, 24). Even at the laboratory scale, there were difficulties in controlling the densification, and careful design of electrodes had to be developed to minimize transient stresses due to inhomogeneous current distributions. A British company, Lucideon (**https://www.lucideon.com/materials-technologies/flash-sintering**), has made progress with prototyping a continuous furnace design to scale for mass production.

1.4. Hydrothermal Sintering

Initially developed in the 1980s for low-temperature sintering of ceramic materials by the Yamasaki group, hydrothermal sintering allowed for the densification of refractory materials such as silica, hydroxyapatite, anatase, and calcium carbonate (25–28). At the time, densification was limited to values of approximately 80% of theoretical values. This process was recently reinvestigated, particularly for the densification of silica, and the possibility of reaching 98% density in quartz was confirmed (29, 30). Hydrothermal sintering has similarities to cold sintering, particularly in the high-pressure and high-water-content end of the processing space spectrum.

1.5. Fast Firing

Fast firing enables high densification and limited grain growth under nonisothermal conditions, as introduced by Brook and colleagues (31, 32). Here, intentional thermal gradients drive diffusion and enhance mass transport to the pores, which are naturally low-temperature localities within the microstructure. With the advancements of roller kiln manufacturing, continuous high-volume mass production by fast firing is being used in a wide range of ceramic industries that include tiles and base-metal multilayer $BaTiO_3$ ceramic capacitors (33–35).

2. COLD SINTERING

In the most generic sense, cold sintering is a densification process that requires two phases: (*a*) a parent powder from which to form a ceramic body and (*b*) a transport phase to facilitate mass transfer to and from the original particles. To date, the majority of examples utilize liquid phases that are water, organic solvent, or alcohol based, but other possibilities should not be excluded. In the ideal limiting case, there is substantial solution between the two phases at low temperatures, a combination of capillarity and applied uniaxial pressure provides the driving case for densification, and the transport phase is fugitive (i.e., most of it escapes the pellet die during densification). In many cases, an ~5% volume fraction of transport phase is sufficient to support densification (49, 50). Among the inorganic materials that have been densified using cold sintering are microwave dielectrics (51–56), ferroelectrics (57, 58), piezoelectrics (59), structural materials (60), Li-ion cathodes (61), solid-state electrolytes (62, 63), semiconductors (64, 65), ceramic

adhesives (66), refractories (67), magnetic ceramics (68), and sputtering target materials (69). While the quantitative role of each material remains to be identified, current data show that particle rearrangement, dissolution, precipitation, and growth participate in the densification process and are affected by the presence and ratio of the transport phase and by the pressing pressure. Modest temperatures (typically in the range of 150°C) promote the kinetics of the dissolution, solute supersaturation, and ultimately precipitation. Liquid evaporation from the densifying powder is also an influential factor.

2.1. Sintering Mechanisms

On the basis of processing similarities, there appears to be an immediate relationship linking cold sintering and liquid phase sintering; the foundational aspects of the latter were identified and parameterized in the original work of Kingery and colleagues (70, 71) and appear relevant to present observations. A summary of the existing cold-sintered material literature makes clear that choosing the transport phase/parent phase combination and understanding the interaction of the two phases are central steps that enable high densities. The critical concerns originate from the multiple forces acting on the system, which ultimately direct the progression to a minimum-free-energy particle ensemble. Liquids and other transport phases can be introduced by mixing them into powders via conventional powder processing techniques or by a vapor transport process.

In one limiting scenario in which the transport phase is a liquid that is present at sufficient volume within a powder compact, the liquid can provide substantial capillary pressure and a transport channel to redistribute material. Work by Randall and colleagues (49) on highly soluble salts like NaCl showed that powder compacts exposed to water will sinter to near-full density with no externally applied pressure. The capillary forces in combination with dissolution-based transport are presumably the densification mechanisms. Kingery and colleagues (70, 71) studied fractional shrinkage due to particle rearrangement as a function of liquid volume fractions and found that values of ~35% are required. The volume fractions used in cold sintering are typically smaller because in most cases one wishes to expel the transport phase. As such, additional drivers, such as the applied uniaxial pressure, are necessary for assisting in rearrangement-based fractional shrinkage.

2.1.1. Solubility-based densification mechanisms. The dissolution and precipitation processes are believed to be important in cold sintering (49, 50, 72). Consider that a green body in the just-pressed state is typically between 60% and 70% of theoretical density. In cold sintering of ZnO, for example, approximately 4 vol% of 0.8 M Zn-acetate solution is effective as a transport phase that can achieve near-full density under pressure and at ~100°C. If all the additional Zn atoms were converted from an acetate to an oxide, and if that new oxide occupied the green body interstitial space, the density would increase by only a few percent. As such, the majority of material redistribution that must occur to approach 100% density must originate from the parent particle surfaces. The available data and observations suggest that such dissolution and precipitation events are the most likely densification mechanism. There is, however, an issue with this model: Dissolution and precipitation are exclusively surface events, and these cannot promote densification, but only coarsening. If surface-to-surface mass transport is the only vehicle available, then it is important to consider the role of stress gradients. In a particle compact under pressure, grain-grain contact points will create local stress concentrations. Consider the simplest model, in which two 10-μm spheres of material with an elastic modulus of 200 GPa are compressed axially at a reasonable pressing pressure of 200 MPa. At the contact point, the Hertzian contact stress is more than 20 GPa. If present in this stress concentration zone, a liquid with finite capacity to dissolve the ceramic grains will create a chemical potential gradient that follows the stress gradient.

Table 2 Various densification rates under the dissolution and precipitation stages in the Kingery model (69)

Morphology	Diffusion rate controlled	Phase boundary reaction controlled
Spherical particles	$\frac{\Delta\ell}{\ell_o} \cong t^{1/3}$	$\frac{\Delta\ell}{\ell_o} \cong t^{1/2}$
Prismatic particles	$\frac{\Delta\ell}{\ell_o} \cong t^{1/6}$	$\frac{\Delta\ell}{\ell_o} \cong t^{1/3}$

We believe that these contact regions provide a driving force for mass transport that creates grain boundary area and enables particle centers to approach.

2.1.2. Densification rates. During the rearrangement stage of liquid phase sintering, the densification rate, as represented by the time dependence of volume and/or linear shrinkage, is represented analytically by Equation 1 (70):

$$\frac{\Delta\ell}{\ell_o} = \frac{1}{3}\frac{\Delta V}{V_o} \sim t^y, \qquad 1.$$

where y is ~1 for particle rearrangement and the second densification stage depends on particle shape and the mass transport mechanism. **Table 2** shows the various scaling rates that parameterize the densification process during the dissolution-precipitation step of liquid phase sintering.

The similarities between cold sintering and liquid phase sintering invite comparison of possible similarities in densification mechanisms. To do so, we adopt the parameterization strategies between density and time developed in the reports of Kingery and colleagues (70, 71) discussed above. To do so, several series of pellets in the pure ZnO system were densified using optimized cold sintering conditions, but the process was arrested before completion. The process was conducted under the same conditions for each pellet: 120°C and two dwell pressures of 530 MPa and 175 MPa. Density was subsequently recorded as a function of duration under pressure and was converted into volume shrinkage versus process time and plotted on log-log axes. **Figure 1** shows the results. Two different regions are immediately evident. To convert data to densification rate,

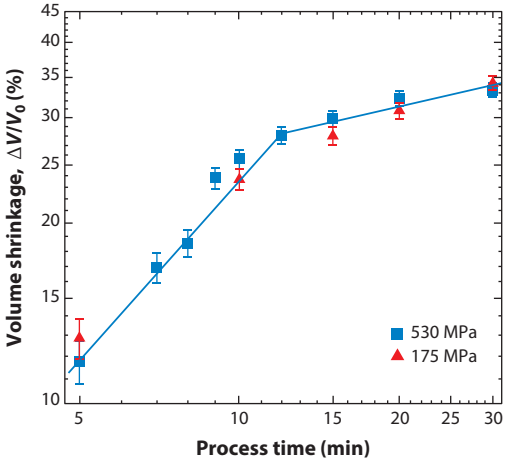

Figure 1

Log-log plots of cold sintering process ZnO pellet volume shrinkage as a function of process time with 0.67 M zinc acetate, with 4% liquid phase content at 120°C, and either at 530 MPa (*blue squares*) or at 175 MPa (*red triangles*) for a typical 30-min process. Individual pellet density was measured at room temperature after cooling to room temperature. The solid line indicates the two slopes of 1 and 1/3.

the initial volume V_o was calculated by fitting the data in the initial region and extrapolating to zero time. In this case, V_o is an approximation representing the volume of the powder compact at the moment when maximum pressure is first achieved. Mass was assumed to be constant for the duration of the process. This is a reasonable approximation since the total additional liquid mass used in the process is less than 5%. For both pressures, there are two regimes of densification rate that we associate primarily with compaction-like and densification mechanisms. Linear fits were separately processed on stage one and stage two for the two data sets.

While there is some scatter in the plot, data points for the initial stage in both series fall on a common line with a slope between 0.95 and 1. This indicates a linear dependence of $\Delta V/V_0$ with time. For the second stage, the volume shrinkage values differ, but both slopes are similar and are approximately 1/3. This distinct two-segment character and the slopes of each line can be interpreted using Kingery and colleagues' (70, 71) model for liquid phase sintering that involves grain rearrangement (stage one) and dissolution-precipitation events (stage two), and this slope could correspond to the diffusion rate–controlled case. These dependences are strikingly similar to those observed for cold sintering. While the evidence is not conclusive, the similarities suggest that cold sintering can also be understood as a multiple-stage process involving phenomena that exhibit rates corresponding to those driven by grain rearrangement and dissolution-precipitation events at short and long times, respectively. It is particularly compelling that the same slopes are present for different applied pressure values, suggesting that similar mechanisms are present over a broad range of densification conditions.

Significantly, the transition from compaction to mass transport remains underexplored. Given the relative slowness of heating in the context of the rapid force application, it is difficult to separate operative phenomena. A full description of this transition is outside the scope of this article, but we include these initial data for this experiment of interest, as these data offer an initial insight into cold sintering mechanisms and illustrate similarities to existing models.

For ZnO pellets prepared using optimized conditions, a 30-min pressure and temperature dwell results in final density values typically above 98% of the theoretical value. When temperature values in the range of 120°C are used, the average grain size changes very little. However, it is important to consider that this is a net effect of existing grains growing slightly larger and a population of newly precipitated grains that are comparatively small. In fact, the sum of both effects pushes the average diameter to slightly smaller values. **Figure 2** shows an example microstructure for ZnO cold sintered with zinc acetate at 120°C at 500 MPa for 30 min. The average particle size for the starting powder was approximately 100 nm.

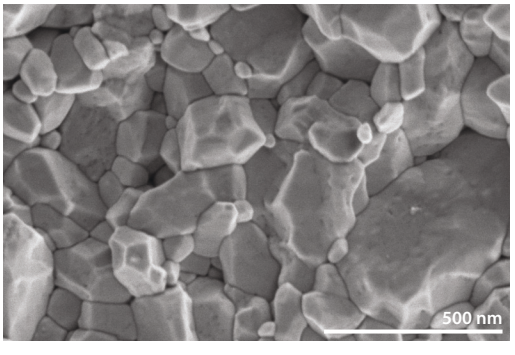

Figure 2

SEM image of a typical ZnO ceramic, cold sintered at 120°C, with a final density greater than 98% of the theoretical value and the initial size averaged to be approximately 160 nm. Details are found in Reference 72.

2.1.3. Liquid-solid interface. The nature of the liquid-solid interface is critical to comprehending the liquid phase sintering process under cold sintering conditions. The interaction of the liquid solvent and the surface of the inorganic material is quite complex; in the case of acetic acid and water, there is an important window of concentration, as this window enables the sufficient kinetics for cold sintering to occur. Techniques such as ReaxFF are being explored to understand the chemical interactions in the grain boundary regions. These interactions are also highly complicated, as there are dynamic chelating reactions, hydrolysis, and cluster formation. The details of these reactions and the associated dynamics are important areas for understanding cold sintering, and these details aid in the determination of the critical solvent selections for each ceramic system to be sintered (73, 74).

Densification experiments using KH_2PO_4 (KDP) and deuterated water reveal additional similarities with liquid phase sintering. In this experiment, KDP ceramics were cold sintered using heavy water (^2H_2O, of D_2O) as the liquid phase. Then, 15-vol% D_2O was added to KDP, was homogenized in a mortar and pestle, and was then cold sintered at 120°C and 350 MPa for 30 min. The initial average grain size was 20 μm, and the final density was >95%. Time-of-flight–secondary ion mass spectroscopy (TOF-SIMS) images were used to image the ceramic microstructure, with contrast originating from the intensity difference between the hydrogen isotopes. The TOF-SIMS and SEM images reveal regions surrounding the grain boundaries that are rich in deuterated hydrogen, as shown in **Figure 3*b–e***. The deuterium-rich zones appear to be several micrometers thick. For comparison, TOF-SIMS images were collected from KDP samples cold sintered with regular water (^1H_2O), and no significant abundance of ^2H was observed. The ^2H distribution in KDP samples cold sintered with D_2O suggests a mechanism by which the transport phase acts upon the original grain surfaces to redistribute material under uniaxial pressure and by which the residual deuterium preferentially resides at the newly formed grain boundaries. These ideas are again consistent with processes similar to liquid phase sintering.

2.1.4. Grain growth. Grain growth is another important aspect of sintering and therefore should be considered (64). Funahashi et al. (64) showed that 10 wt% of 1 M of the acetic acid transport phase could densify ZnO at temperatures between 120°C and 305°C, at a pressure of 350 MPa, and for times ranging from 30 min to 5 h. The starting powder had an average ZnO particle size of 200 nm. It is well known that the grain size exponent N is proportional to the sintering time under isothermal conditions for materials with constant densities, in accordance with Equation 2:

$$G^N - G_0^N = tK_0 \exp Q/RT, \qquad 2.$$

where G_0 is the initial grain size, t is the sintering time, N is the kinetic grain growth exponent, K_0 is a constant, Q is the apparent activation energy for grain growth, R is the gas constant, and T is the absolute temperature. Equation 2 can, in turn, be simplified in Equation 3 to

$$\log G = (1/N)\log t + (1/N)[\log K_0 - 0.434(Q/RT)]. \qquad 3.$$

Then, from the Arrhenius plots between the power of the grain size and $1/T$, the activation energy for grain coarsening, Q, can be estimated from Equation 4:

$$\log(G^3/t) = \log K_0 - 0.434(Q/RT). \qquad 4.$$

This analysis and treatment were applied to ZnO as described above at an isothermal condition of 305°C. **Figure 4** shows plots of the grain size data for sintering time (panel *a*) and an Arrhenius plot of the cube of the grain size at each sintering temperature (panel *b*). The grain size increased

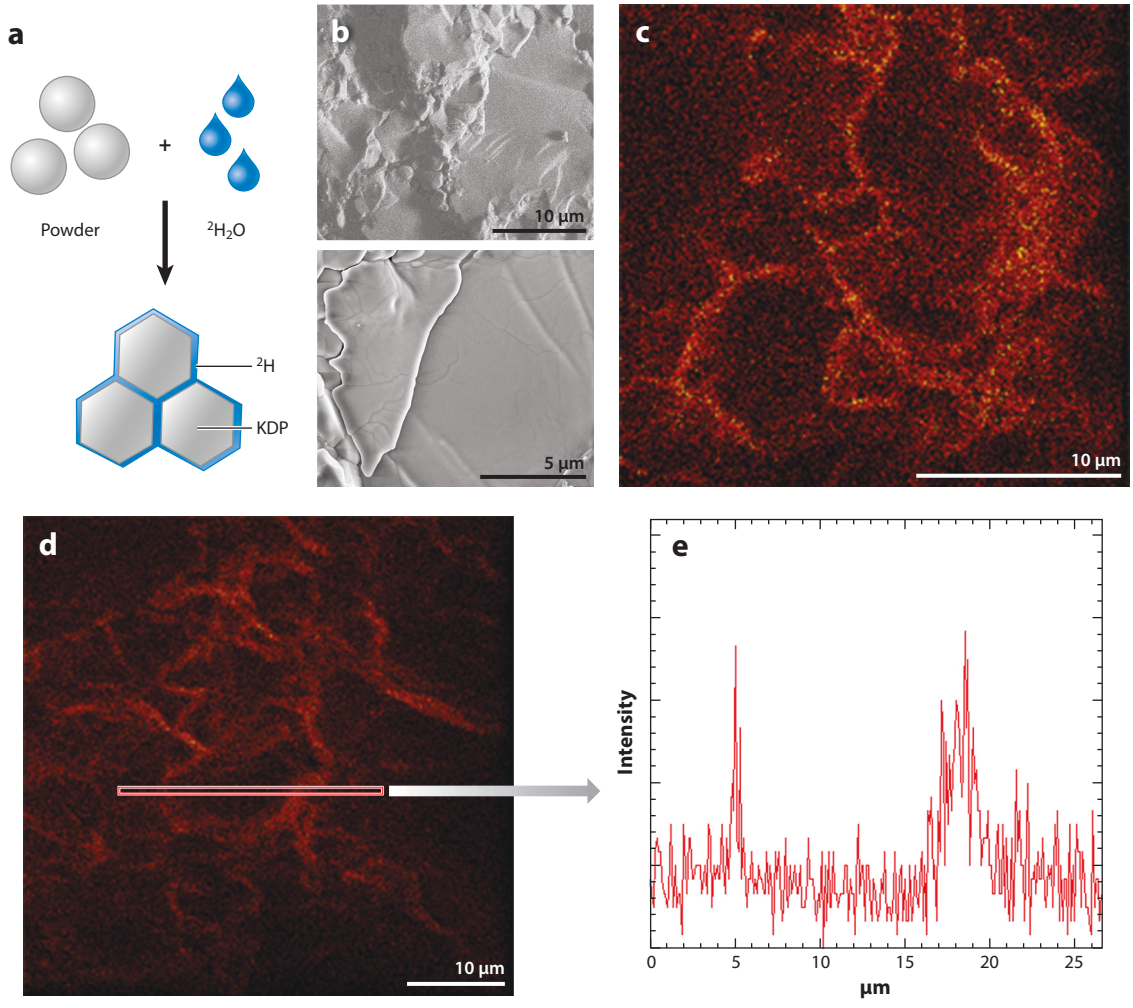

Figure 3

Time-of-flight–secondary ion mass spectrometry (TOF-SIMS) analysis of KH_2PO_4 (KDP) ceramics cold sintered at 120°C with heavy water (^2H_2O). (*a*) Schematic showing the core-shell structure of KDP cold sintered with ^2H_2O. (*b*) SEM images of fracture surfaces of cold-sintered KDP. (*c*,*d*) TOF-SIMS images of cold-sintered KDP at different magnifications. (*e*) Line scan of the ^2H map from panel *d*.

with the sintering time, demonstrating grain coarsening under the cold sintering process. The kinetic grain growth exponent was determined as $N \sim 3$. This value is consistent with reports for liquid phase sintering (1).

If one assumes a similar sintering mechanism between 126°C and 305°C and takes into account that the density is essentially constant at ~98%, the activation energy of grain growth is then calculated from the slope of **Figure 4*b*** and is found to be 43 kJ/mol. Activation energy values for conventionally sintered ZnO are reported to be greater than 200 kJ/mol, which is substantially larger than has been previously observed (64). At this point, we have not fully considered the effective activation energetics of densification, but it is sensible to predict and expect lower energy barriers for all stages of densification under cold sintering.

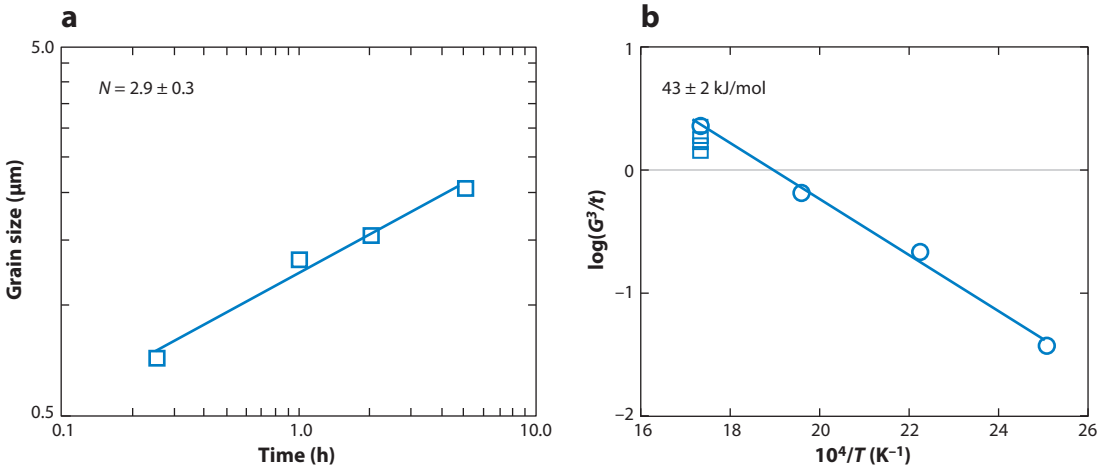

Figure 4

(*a*) Plot of the isothermal log-log grain growth showing a power exponent of $N \sim 3$ at 305°C. (*b*) Arrhenius plot of the grain growth process with an activation energy of 43 kJ/mol, which is much lower than the reported conventional energies of 200 kJ/mol for ZnO cold sintered between 70°C and 305°C and for times of 30 min to 6 h. The squares correspond to those in panel *a*, while the circles relate to a new series of experiments at different temperatures. Adapted with permission from Reference 64. Copyright 2017, John Wiley and Sons.

2.2. Different Pathways Under Cold Sintering Conditions

A number of different pathways can be considered with cold sintering, as shown in **Figure 5**. In the simplest case, a solvent congruently dissolves the surface atomic species; the kinetics of this dissolution can depend on the specific chemistry of the liquid, the inorganic material, the surface area of the particles, and the temperature. The applied pressure used during cold sintering causes high-stress regions in the powder compact. At the contact points between neighboring grains, the local stress can exceed gigapascals of pressure (75–77), and this pressure can accelerate the dissolution process. The supersaturated solution will precipitate when a strain, temperature, or curvature gradient is encountered, or the solution will precipitate with time if the solvent phase is lost by extrusion or evaporation. In some cases, especially when evaporation is rapid, we observe solute gelation and a subsequent disordered phase within the grain boundaries. Examples of interest include $Na_2Mo_2O_7$ and V_2O_5 (65, 78). **Figure 6** shows a $Na_2Mo_2O_7$ ceramic microstructure cold sintered at 120°C under 350 MPa for 15 min. As seen in **Figure 6*a–c***, there is a thick and highly disordered intergranular phase at some grain boundaries, and the grain termination to these regions is highly crystalline and abrupt. Nanometer-sized nuclei are observed on/near some crystal surfaces within the disordered interface region. The interfacial rough terrace structures of cold-sintered $Na_2Mo_2O_7$ ceramics suggest the formation of nonequilibrated interfaces. While an intergranular phase is present at some interfaces, abrupt grain boundaries are observed in most regions, as shown in **Figure 6*d***.

Incongruent dissolution and cold sintering are more complex than first appreciated in 2016, when we considered that if a material experiences incongruent dissolution, then the residual amorphous surfaces at the liquid-solid interface limit precipitation (57). In cases such as $BaTiO_3$, observations are consistent (57). However, in systems like LAGP ($Li_{1.5}Al_{0.5}Ge_{1.5}P_3O_{12}$), there is preferential dissolution of Li^+ and PO_4, but there is still densification under cold sintering (62, 79). As such, there must be additional interactions between surface structures and solvent species, with more complicated kinetics of dissolution and precipitation that participate in a dynamic green

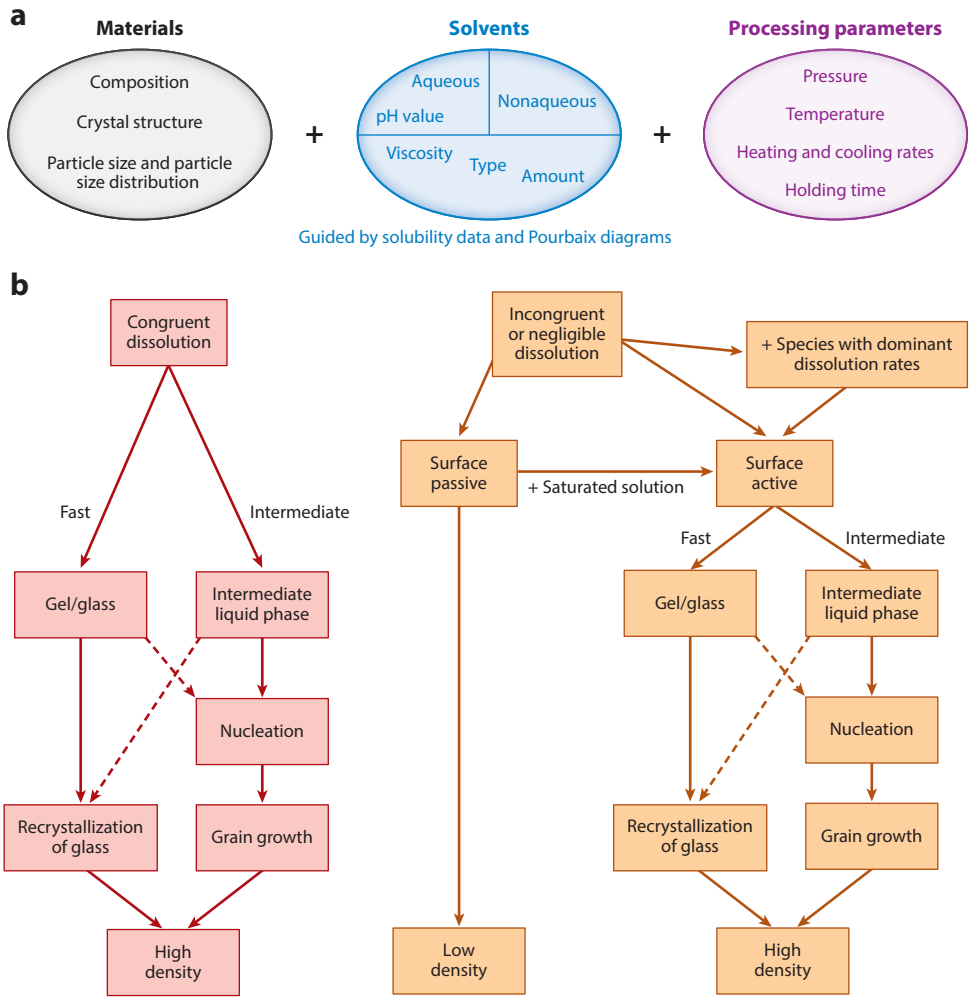

Figure 5

Flowchart showing (*a*) the key synthesis parameters and (*b*) different pathways that cold sintering can take for different materials under different conditions to densify. In panel *b*, the solid lines are typical pathways; the dashed lines denote pathways that are less common but that have been observed.

body with stress and curvature gradients (80). Using solvents that are rich in the species that have the dominant dissolution rates can limit the driving forces of incongruent dissolution processes, and using these designed solvents can aid in stoichiometric control at the particle surface, enabling densification (58, 59).

Incongruent dissolution and/or crystallization under cold sintering conditions can produce second phases that are deleterious to properties, such as limiting ionic or electronic conduction (62, 63) and, in the case of high-permittivity dielectrics, decreasing the permittivity from low-permittivity interfacial regions (57). In conventional ceramic liquid phase sintering, one may expect some interfacial atomic disorder via nanoscale intergranular phase formation (81). Clarke (81) proposed that the intergranular glass phases reflect a balance between van der Waals attraction and a resistance to the deformation of glass boundaries. Even in conventional sintering, the details

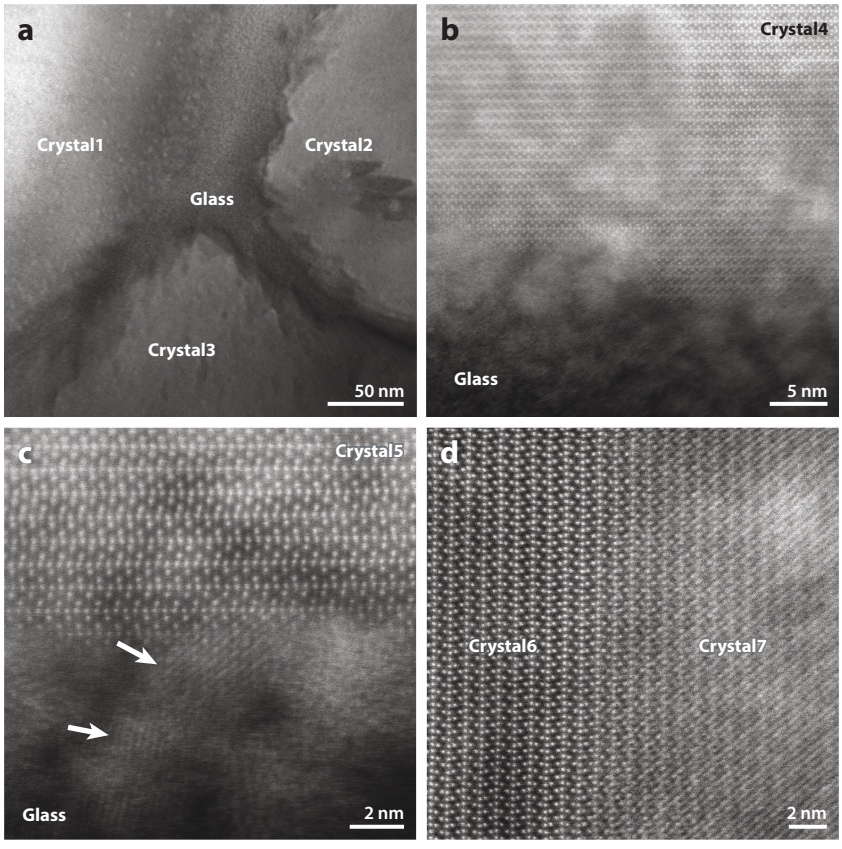

Figure 6

(*a*) Bright-field TEM and (*b–d*) HAADF-STEM images of $Na_2Mo_2O_7$ ceramics cold sintered at 120°C at different stages of microstructural development. (*a*) Grain boundaries showing the terrace steps. (*b*) Interface of crystalline grains and thick glassy interphases. (*c*) $Na_2Mo_2O_7$ nanometer-sized nuclei on the crystal surface within a glassy interface region. The white arrows point out the $Na_2Mo_2O_7$ nanometer-sized nuclei. (*d*) Highly developed clean interfaces between adjacent grains.

of these intergranular phases depend on many different factors, including solute segregation, residual glass, and sintering aids (81–83). Transmission electron microscopy observations show that there is an equilibrium thickness of these intergranular boundaries. Such intergranular films are now considered as a subgroup of a broader description of grain boundaries involving quasi-liquid interfacial films; such boundaries are referred to as complexions. The details of the atomic disorder as grains transition across these all-important interphases can systematically change with sintering temperature, as has been demonstrated across four different disordered complexion scenarios in a 400°C window between 1,400°C and 1,800°C in α-alumina (83). We include these intergranular glass phase and complexation concepts because analogs may exist for cold sintering. While we do not have data to support or refute their presence, as we interpret new data sets, we should include these as open mechanistic possibilities.

Colloidal interparticle forces have been related to the sintering process in liquid phases and sintering in vitreous media. We suspect that such forces also influence cold sintering. A common consideration in colloid and sintering science is surface energy minimization that is brokered by

the balance between interactive forces that control the colloid interparticle separation and grain boundary creation. A similar interplay between forces should be considered in cold sintering. Van der Waals attraction operates at short distances, while at longer distances, electrostatic forces, controlled by surface charge and distribution of counterions in the adjacent liquid, predominate. In the cold sintering context, in which liquid volume fractions are low, by necessity the liquid will have high concentrations of ions that will provide high local osmotic pressures. Such conditions may, in some cases, aid in particle sliding under uniaxial pressure. If local particle ensembles are rigid, the high osmotic pressure will promote solute ion diffusion into triple-point regions where higher concentrations will cause precipitation, thereby reducing the solid-vapor or solid-liquid interface area and reducing the overall free energy. Under the cold sintering process, solvents are selected to allow high ionic solubility exchanges to occur during densification. With dissolution at surfaces, both cationic and ionic species at the surfaces of the particles can occur, and the concentration can be close to supersaturation, especially with the transient evaporation of the solvent. Precipitates can occur homogeneously in the liquids and heterogeneously on the surfaces of the particles. Furthermore, the nature and role of osmotic pressure and other electrokinetic processes, such as diffusiophoresis, need to be considered under cold sintering processes.

3. OPPORTUNITIES AND CHALLENGES

3.1. Cold-Sintered Composites

It is of interest to develop composite materials that possess better properties than the individual components. However, it is typically challenging to cosinter ceramics with polymers and nanoparticles due to incompatibilities at high temperatures. The low thermal budgets for cold sintering provide a new opportunity landscape to cosinter a diverse material selection.

In the case of polymers, we have demonstrated a number of examples of dense ceramic-polymer composites with intergranular polymer distributions (79, 84), summarized in **Table 3**. These reports illustrate how the electrical, mechanical, and thermal properties of ceramics can be designed using polymers as fillers through the cold sintering process (79, 84). **Figure 7*a*** shows a representative example set of different types of ceramic composites enabled by cold sintering, including polymers, carbon nanofibers, and 2D nanoparticles. **Figure 7*b*** shows the ability to cold sinter highly dense Li electrolytes (LAGP) with 95% ceramic and 5% polyethylene oxide. Panels *c* to *f* of **Figure 7** show high-resolution TEM images of the intergranular regions with polytetrafluoroethylene (PTFE), carbon nanofibers, and MXene, respectively. For the cases of ZnO and PTFE, we form a composite structure in which semiconducting grains are jacketed in an insulating layer to produce a varistor-like response. The current-voltage response is highly nonlinear, with a larger electrical breakdown strength per grain boundary (85).

Nanoparticle fillers are another important new opportunity for grain boundary design. With a major expansion of nanoparticles over the last 30 years, there are now very interesting opportunities to integrate them into ceramics, ceramic-polymer composites, and ceramic-metal composites. Conventional limitations to particle-nanoparticle composites include chemical reactivity, decomposition, particle coarsening, and grain boundary pinning. With cold sintering, several of these concerns are obviated, and a spectrum of ceramic nanocomposites can be densified. In many instances, the electrical and mechanical properties of ceramics are improved with even a few volume percent of nanoparticles. Representative examples of such composites are demonstrated across a number of new systems, and a subset of these results are summarized in **Table 4**.

Nanomaterials with rationally engineered grain boundary phases produced by cold sintering provide one example of many composite opportunities. We can envision a new era of nanocomposites for which integration is unencumbered by formulation. One can now consider a dense

Table 3 Examples of cold-sintered ceramic-polymer composites

Matrix ceramic	Grain boundary polymer	Liquid	Sintering condition	Relative density (%)	Property design
LAGP ($Li_{1.5}Al_{0.5}Ge_{1.5}P_3O_{12}$) (Li-ion electrolyte) (62, 79)	PVDF-HFP (polyvinylidene fluoride-*co*-hexafluoropropylene) and $LiPF_6$ (lithium hexafluorophosphate)	Deionized (DI) water	Temp: 120°C Pressure: 400 MPa Time: 1 h	80–88	Reducing grain boundary ionic resistance in Li-ion electrolytes for all-solid-state batteries
V_2O_5 (semiconductor) (65, 79, 86)	PEDOT:PSS [poly(3,4-ethylenedioxythiophene): polystrene sulfonate]	DI water	Temp: 120°C Pressure: 350 MPa Time: 20–30 min	93–96	Reducing electronic resistance at the grain boundary for negative-temperature-resistance sensors
ZnO (semiconductor) (85)	PTFE (polytetrafluoroethylene)	Acetic acid	Temp: 285°C Pressure: 300 MPa Time: 1 h	92–97	Developing resistive barriers at grain boundaries for nonlinear conduction for varistors
$Na_2Mo_2O_7$ (microwave dielectric) (78)	PEI (polyetherimide)	DI water	Temp: 120°C Pressure: 350 MPa Time: 20 min	94–98	Improving grain boundary resistance and breakdown strength for electronic substrates
LMO (Li_2MoO_4) (51, 79)	PTFE	DI water	Temp: 120°C Pressure: 350 MPa Time: 15–20 min	92–98	Designing microwave and elastic properties

heterogeneous monolith containing polymers, ceramics, and metals. We refer to this construction as a polycermet and are excited to explore what properties can evolve from this diverse mixture of phases.

3.2. Potential Hybrid Cold Sintering Processes

As we contemplate a future transition of cold sintering from the laboratory, we must consider avenues for compatibility with scaled manufacturing. Despite the early understanding of cold sintering mechanisms, it is not premature to consider this technological challenge. One area of investment should focus on lowering the applied pressure. Currently, many systems require pressing pressures in the range between 100 MPa and 300 MPa. Such pressures are easily accessed in laboratory-scale dies, but larger parts require forces that push the limits of available instrumentation. Important clues in the literature identify opportunities. For example, applying electric fields, as with SPS and flash sintering, offers potential densification acceleration possibilities for cold

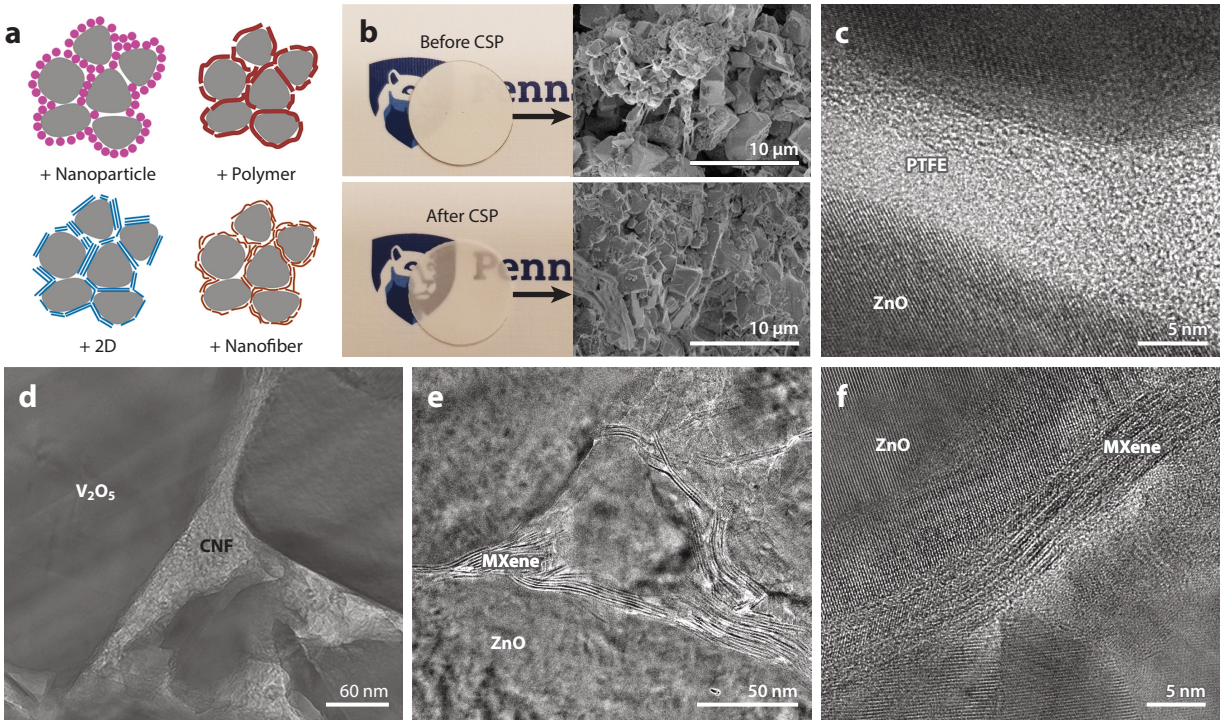

Figure 7

Examples of incorporation of nanomaterials into bulk ceramics under a cold sintering process (CSP). (*a*) Schematic of ceramic-based composites with different fillers. (*b*) Photos and SEM images of LAGP-PEO ($Li_{1.5}Al_{0.5}Ge_{1.5}P_3O_{12}$–polyethylene oxide) composites before and after cold sintering at 150°C. (*c–f*) TEM images of (*c*) ZnO-polytetrafluoroethylene (PTFE) (ceramic-polymer), (*d*) V_2O_5-CNF (ceramic–carbon nanofiber), and (*e*,*f*) ZnO-MXene (ceramic–2D material) nanocomposites cold sintered at 285°C, 120°C, and 300°C, respectively, showing the presence of polymer/CNF/2D material at the ceramic grain boundaries.

Table 4 Examples of ceramic-based composites with nanoparticle fillers

Ceramic	Nanofiller	Liquid	Sintering condition	Relative density (%)	Property design
$LiFePO_4$ (87)	Carbon fibers	LiOH solution	Temp: 180°C Pressure: 240 MPa Holding time: 10 min	70–89	Enhanced mixed electrical/ionic conduction for faster electrochemical intercalation in Li cathodes
ZnO (88)	MXene $Ti_3C_2T_x$ 2D powders	1.5 M acetic acid	Temp: 300°C Pressure: 250 MPa Holding time: 1 h	92–99	Enhanced mechanical and electronic properties
V_2O_5 (89)	Carbon nanotubes/ fibers	Deionized water	Temp: 120°C Pressure: 350 MPa Holding time: 20 min	84–95	Enhanced conductivity
TiO_2	Metal organic frameworks	Not available	Not available	Not available	Enhanced catalyst activity
$CaCO_3$	Nanocellulose	Not available	Not available	Not available	Structural properties

Table 5 Potential hybrid cold sintering processes

Method	System	Coupling mechanism
Spark plasma sintering (20)	ZnO + acetic acid vapor	Joule heating and fast heating
Electric field–assisted sintering (90)	ZnO + water vapor	Joule heating and fast heating
Microwave sintering	ZnO + acetic acid	Joule heating and fast heating

sintering. The work of Luo and colleagues (90) shows the ability to sinter ZnO, when exposed to an applied field, with a small quantity of water and an extremely small applied pressure to full density in a matter of seconds. It is similarly interesting to consider assisting cold sintering with microwave and acoustic energy with the goal of reducing the pressure and time budgets. **Table 5** summarizes potential hybrid cold sintering processes.

3.3. Key Needs from the Science and Engineering Viewpoint

The basic science of cold sintering is just beginning, but fundamental thermodynamics provide insights into understanding the driving forces that promote densification (91, 92). Following convention, Equation 5 quantifies the free energy of a particle compact in terms of surface and interface free energies. The $\gamma \mathrm{d}A$ term is the driving force for particle coarsening; increasing particle size reduces surface area and thus surface energy but lowers the driving force for densification.

$$\Delta G = \gamma \mathrm{d}A + A\mathrm{d}\gamma. \qquad 5.$$

In contrast, the $A\mathrm{d}\gamma$ term is the driving force for densification; increasing grain boundary area eliminates the solid-vapor interface area and reduces the overall free energy while bringing particle centers together. Again, following convention, $\mathrm{d}\gamma$ can happen only via bulk transport, which cannot occur in cold sintering since there is insufficient temperature to move vacancies, but densification does happen.

It is sensible to conjecture that surface-only processes, such as dissolution and precipitation, combined with large stress gradients at particle-particle contacts provide a directional mass transport from high to low stress, which would be from the center to the periphery of interparticle contacts. This assisted surface transport may be related to the high pressures needed for cold sintering and directs our experiments and approaches to lowering them.

The interaction between the parent phase and the transport phase offers a more diverse set of transport phenomena, on a case-by-case basis, that may change the energy landscape and provide additional experimental options. For example, in systems showing rapid dissolution and reprecipitation, such as $Na_2Mo_2O_7$, higher γ particle surfaces become rough at the atomic scale, as evidenced by the microstructural data in **Figure 6**. This roughness increase may lower the tendency for coarsening, which in turn reduces the competition against minimizing $A\mathrm{d}\gamma$ and compact densification.

Significant work is required to drive the detailed fundamental understanding of cold sintering and to enable the incorporation of this technique into manufacturing processes. This article partially addresses the current status of cold sintering as well as some of the key science and engineering needs, as summarized in **Table 6**, for advancing fundamental understanding and implementation of the process. One example of these critical needs is the scientific guidance of solvent selection. We see that in model systems, such as ZnO, there is a critical concentration of acetic acid needed for densification; ZnO can also sinter with other organic acids, such as formic and citric acids, but there are differences in the kinetics and densification. If a better understanding of the solvent-particle interface chemistry could be obtained by more sophisticated scientific principles

Table 6 Key fundamental and engineering needs for cold sintering

Fundamental research needs for cold sintering	Engineering research needs for cold sintering
■ Quantify the key kinetics and grain growth parameters in various systems	■ Demonstrate new types of ceramics and ceramic composites with engineered properties
■ Develop scientific guidance of solvent selection to drive cold sintering	■ Develop education and training of cold sintering methodologies
■ Design new nanocomposites and grain boundaries	■ Develop powders for polymer, ceramic, and metal composites for designing new composites and integrated materials
■ Structurally characterize and model interfaces in the early stages of sintering, both in situ and ex situ	■ Develop larger-scale sintering pressure-temperature fixtures for better processes
■ Develop mechanisms underpinning hybrid-assisted cold sintering	■ Develop a continuous process for cold sintering
■ Contrast properties of cold-sintered materials with properties of conventionally sintered materials	

than relative dissolution kinetics and precipitation routes, then advancements in the process would be accelerated across more materials. We suspect such understanding would lead to densification at lower temperatures and applied pressures. Further in situ and ex situ characterization and related modeling of the interface behavior could be used to gain this needed insight (93, 94). Other improvements along these lines may be possible by adding other physical energies to assist in cold sintering, and such approaches are already showing great merit in simple model systems (72).

Ultimately, for cold sintering to have a strong impact on the technology community, a more in-depth understanding of the mechanisms and process factors is necessary. Basic demonstrations of proof of concept in different ceramic compositions and of new concepts in nanocomposites have been shown, but the large-scale manufacturing of such materials and devices will demonstrate the true importance of cold sintering, both in footprint and in volume. This development will require the education of industrial partners and a willingness of companies to consider the transition and scaling of a batch process to a continuous process. There is somewhat of a risk to any company with such a major change to production methodologies when considering the financial aspects, training, and knowledge accumulation of the product development. However, forces outside the basic academic arena are driving unique designs of new products, faster and lower-energy processes, and emissions control in production, which could support advancement and implementation of new process technologies, such as cold sintering and its competitors. There is also the possibility of learning from other present mass production techniques that may need only minor changes; one possibility is in the polymer lamination manufacturers (95). Finally, in these early days, there is no one strategic plan for this discovery, but as activities across the world in cold sintering are moving forward and as different groups get involved, the issues outlined in **Table 6** will advance and evolve.

DISCLOSURE STATEMENT

The authors are not aware of any affiliations, memberships, funding, or financial holdings that might be perceived as affecting the objectivity of this review.

ACKNOWLEDGMENTS

This work was supported in part by National Science Foundation (NSF) DMR-1728634, AFOSR FA9550-16-1-0429, ARPA-E DE-AR0000766, and the NSF as part of the Center for Dielectric Studies under grants IIP-1361571 and 1361503. We also acknowledge the use of the facilities at the Materials Characterization Laboratory and its staff. **Figure 2** comes from work performed at

the Analytical Instrumentation Facility (AIF), affiliated with the National Nanotechnology Coordinated Infrastructure (NNCI) at North Carolina State University, which is supported by the state of North Carolina and the NSF (award number ECCS-1542015).

LITERATURE CITED

1. German RM. 1996. *Sintering Theory and Practice*. New York: Wiley
2. Vandiver PB, Soffer O, Klima B, Svoboda J. 1989. The origins of ceramic technology at Dolni Věstonice, Czechoslovakia. *Science* 246(4933):1002–8
3. German RM. 2014. *Sintering: From Empirical Observations to Scientific Principles*. Oxford, UK: Elsevier
4. Coble RL. 1961. Sintering crystalline solids. I. Intermediate and final state diffusion models. *J. Appl. Phys.* 32(5):787–92
5. Coble RL. 1961. Sintering crystalline solids. II. Experimental test of diffusion models in powder compacts. *J. Appl. Phys.* 32(5):793–99
6. Kingery WD, Berg M. 1955. Study of the initial stages of sintering solids by viscous flow, evaporation-condensation, and self-diffusion. *J. Appl. Phys.* 26(10):1205–12
7. Frenkel JJ. 1945. Viscous flow of crystalline bodies under the action of surface tension. *J. Phys.* 9:385
8. Lee SH, Kupp ER, Stevenson AJ, Anderson JM, Messing GL, et al. 2009. Hot isostatic pressing of transparent Nd:YAG ceramics. *J. Am. Ceram. Soc.* 92(7):1456–63
9. Rossi RC, Fulrath RM. 1965. Final stage densification in vacuum hot-pressing of alumina. *J. Am. Ceram. Soc.* 48(11):558–64
10. Wu WW, Zhang GJ, Kan YM, Wang PL. 2006. Reactive hot pressing of ZrB_2-SiC-ZrC ultra high-temperature ceramics at 1800°C. *J. Am. Ceram. Soc.* 89(9):2967–69
11. Wang W, Fu Z, Wang H, Yuan R. 2002. Influence of hot pressing sintering temperature and time on microstructure and mechanical properties of TiB_2 ceramics. *J. Eur. Ceram. Soc.* 22(7):1045–49
12. Zhang G, Deng Z, Kondo N, Yang J, Ohji T. 2000. Reactive hot pressing of ZrB_2-SiC composites. *J. Am. Ceram. Soc.* 83(9):2330–32
13. Jaeger RE, Egerton L. 1962. Hot pressing of potassium-sodium niobates. *J. Am. Ceram. Soc.* 45(5):209–13
14. Agrawal D. 2006. Microwave sintering of ceramics, composites, and metallic materials, and melting of glasses. *Trans. Indian Ceram. Soc.* 65(3):129–44
15. Brosnan KH, Messing GL, Agrawal DK. 2003. Microwave sintering of alumina at 2.45 GHz. *J. Am. Ceram. Soc.* 86(8):1307–12
16. Heuguet R, Marinel S, Thuault A, Badev A. 2013. Effects of the susceptor dielectric properties on the microwave sintering of alumina. *J. Am. Ceram. Soc.* 96(12):3728–36
17. Breval E, Cheng JP, Agrawal DK, Gigl P, Dennis M, et al. 2005. Comparison between microwave and conventional sintering of WC/Co composites. *Mater. Sci. Eng. A* 391:285–95
18. Shen Z, Johnsson M, Zhao Z, Nygren M. 2002. Spark plasma sintering of alumina. *J. Am. Ceram. Soc.* 85(8):1921–27
19. Manière C, Durand L, Chevallier G, Estournès C. 2018. A spark plasma sintering densification modeling approach: from polymer, metals to ceramics. *J. Mater. Sci.* 53(10):7869–76
20. Gonzalez-Julian J, Neuhaus K, Bernemann M, Pereira da Silva J, Laptev A, et al. 2018. Unveiling the mechanisms of cold sintering of ZnO at 250°C by varying applied stress and characterizing grain boundaries by Kelvin Probe Force Microscopy. *Acta Mater.* 144:116–28
21. Herisson de Beauvoir T, Sangregorio A, Cornu I, Elissalde C, Josse M. 2018. Cool-SPS: an opportunity for low temperature sintering of thermodynamically fragile materials. *J. Mater. Chem. C* 6(9):2229–33
22. Herisson de Beauvoir T, Molinari F, Chung-Seu UC, Michau D, Denux D, Josse M. 2018. Densification of $MnSO_4$ ceramics by Cool-SPS: evidences for a complex sintering mechanism and magnetoelectric coupling. *J. Eur. Ceram. Soc.* 38(11):3867–74
23. Cologna M, Rashkova B, Raj R. 2010. Flash sintering of nanograin zirconia in <5 s at 850°C. *J. Am. Ceram. Soc.* 93(11):3556–59
24. Cologna M, Francis JSC, Raj R. 2011. Field assisted and flash sintering of alumina and its relationship to conductivity and MgO-doping. *J. Eur. Ceram. Soc.* 31(15):2827–37

25. Yanagisawa K, Nishioka M, Ioku K, Yamasaki N. 1993. Densification of silica gels by hydrothermal hot-pressing. *J. Mater. Sci. Lett.* 12:1073–75
26. Yamasaki N, Kai T, Nishioka M, Yanagisawa K, Ioku K. 1990. Porous hydroxyapatite ceramics prepared by hydrothermal hot-pressing. *J. Mater. Sci. Lett.* 9:1150–51
27. Yanagisawa K, Ioku K, Yamasaki N. 1997. Formation of anatase porous ceramics by hydrothermal hot-pressing of amorphous titania spheres. *J. Am. Ceram. Soc.* 80(5):1303–6
28. Yamasaki N, Weiping T, Jiajun K. 1992. Low-temperature sintering of calcium carbonate by a hydrothermal hot-pressing technique. *J. Mater. Sci. Lett.* 11:934–36
29. Ndayishimiye A, Largeteau A, Mornet S, Duttine M, Dourges M-A, et al. 2018. Hydrothermal sintering for densification of silica. Evidence for the role of water. *J. Eur. Ceram. Soc.* 38:1860–70
30. Ndayishimiye A, Largeteau A, Prakasam M, Pechev S, Dourges MA, Goglio G. 2018. Low temperature hydrothermal sintering process for the quasi-complete densification of nanometric α-quartz. *Scr. Mater.* 145:118–21
31. Brook RJ. 1982. Fabrication principles for the production of ceramics with superior mechanical properties. *Proc. Br. Ceram. Soc.* 32:7–15
32. Harmer MP, Brook RJ. 1981. Fast firing—microstructural benefits. *Trans. J. Br. Ceram. Soc.* 80(5):147–48
33. Garcia DE, Klein AN, Hotza D. 2012. Advanced ceramics with dense and fine-grained microstructures through fast firing. *Rev. Adv. Mater. Sci.* 30:273–81
34. Polotai AV, Fujii I, Shay DP, Yang G-Y, Dickey EC, Randall CA. 2008. Effect of heating rates during sintering on the electrical properties of ultra-thin Ni-$BaTiO_3$ multilayer ceramic capacitors. *J. Am. Ceram. Soc.* 91(8):2540–44
35. Polotai AV, Yang GY, Dickey EC, Randall CA. 2007. Utilization of multiple-stage sintering to control Ni electrode continuity in ultrathin Ni-$BaTiO_3$ multilayer capacitors. *J. Am. Ceram. Soc.* 90(12):3811–17
36. Xue LA, Chen Y, Gilbart E, Brook RJ. 1990. The kinetics of hot-pressing for undoped and donor-doped $BaTiO_3$ ceramics. *J. Mater. Sci.* 25:1423–28
37. Martirena H, Burfoot J. 1974. Grain-size and pressure effects on dielectric and piezoelectric properties of hot-pressed PZT-5. *Ferroelectrics* 7(1–4):151–52
38. Katz JD. 1992. Microwave sintering. *Annu. Rev. Mater. Sci.* 22:153–70
39. McNeal MP, Jang SJ, Newnham RE. 1998. The effect of grain and particle size on the microwave properties of barium titanate ($BaTiO_3$). *J. Appl. Phys.* 83(6):3288–97
40. Takeuchi T, Suyama Y, Sinclair DC, Kageyama H. 2001. Spark-plasma-sintering of fine $BaTiO_3$ powder prepared by a sol-crystal method. *J. Mater. Sci.* 36:2329–34
41. Baraki R, Schwarz S, Guillon O. 2012. Effect of electrical field/current on sintering of fully stabilized zirconia. *J. Am. Ceram. Soc.* 95(1):75–78
42. Olevsky EA, Rolfing SM, Maximenko AL. 2016. Flash (ultra-rapid) spark-plasma sintering of silicon carbide. *Sci. Rep.* 6(1):33408
43. Omori M. 2000. Sintering, consolidation, reaction and crystal growth by the spark plasma system (SPS). *Mater. Sci. Eng. A* 287:183–88
44. Karakuscu A, Cologna M, Yarotski D, Won J, Francis JSC, et al. 2012. Defect structure of flash-sintered strontium titanate. *J. Am. Ceram. Soc.* 95(8):2531–36
45. Yanagisawa K, Ioku K, Yamasaki N. 1995. Post-sintering of anatase compact prepared by hydrothermal hot-pressing. *J. Mater. Sci. Lett.* 14(3):161–63
46. Somiya S. 1984. Hydrothermal preparation and sintering of fine ceramic powders. *Mater. Res. Soc. Symp. Proc.* 24:255–71
47. Vakifahmetoglu C, Anger JF, Atakan V, Quinn S, Gupta S, et al. 2016. Reactive hydrothermal liquid-phase densification (rHLPD) of ceramics—a study of the $BaTiO_3$[TiO_2] composite system. *J. Am. Ceram. Soc.* 99(12):3893–901
48. Polotai A, Breece K, Dickey E, Randall C, Ragulya A. 2005. A novel approach to sintering nanocrystalline barium titanate ceramics. *J. Am. Ceram. Soc.* 88(11):3008–12
49. Guo J, Guo H, Baker AL, Lanagan MT, Kupp ER, et al. 2016. Cold sintering: a paradigm shift for processing and integration of ceramics. *Angew. Chem. Int. Ed.* 55(38):11457–61

50. Maria JP, Kang X, Floyd RD, Dickey EC, Guo H, et al. 2017. Cold sintering: current status and prospects. *J. Mater. Res.* 32(17):3205–18
51. Guo J, Baker AL, Guo H, Lanagan M, Randall CA. 2017. Cold sintering process: a new era for ceramic packaging and microwave device development. *J. Am. Ceram. Soc.* 100(2):669–77
52. Induja IJ, Sebastian MT. 2018. Microwave dielectric properties of cold sintered Al_2O_3-NaCl composite. *Mater. Lett.* 211:55–57
53. Wang D, Zhou D, Zhang S, Vardaxoglou Y, Whittow WG, et al. 2018. Cold-sintered temperature stable $Na_{0.5}Bi_{0.5}MoO_4$-Li_2MoO_4 microwave composite ceramics. *ACS Sustain. Chem. Eng.* 6:2438–44
54. Hong WB, Li L, Cao M, Chen XM. 2018. Plastic deformation and effects of water in room-temperature cold sintering of NaCl microwave dielectric ceramics. *J. Am. Ceram. Soc.* 101(9):4038–43
55. Kahari H, Teirikangas M, Juuti J, Jantunen H. 2016. Room-temperature fabrication of microwave dielectric Li_2MoO_4-TiO_2 composite ceramics. *Ceram. Int.* 42(9):11442–46
56. Kahari H, Teirikangas M, Juuti J, Jantunen H. 2014. Dielectric properties of lithium molybdate ceramic fabricated at room temperature. *J. Am. Ceram. Soc.* 97(11):3378–79
57. Guo H, Baker A, Guo J, Randall CA. 2016. Cold sintering process: a novel technique for low-temperature ceramic processing of ferroelectrics. *J. Am. Ceram. Soc.* 99(11):3489–507
58. Guo H, Baker A, Guo J, Randall CA. 2016. Protocol for ultralow-temperature ceramic sintering: an integration of nanotechnology and the cold sintering process. *ACS Nano* 10(11):10606–14
59. Wang D, Guo H, Morandi CS, Randall CA, Trolier-McKinstry S. 2018. Cold sintering and electrical characterization of lead zirconate titanate piezoelectric ceramics. *APL Mater.* 6:016101
60. Bouville F, Studart AR. 2017. Geologically-inspired strong bulk ceramics made with water at room temperature. *Nat. Commun.* 8:14655
61. Seo JH, Guo J, Guo H, Verlinde K, Heidary DSB, et al. 2017. Cold sintering of a Li-ion cathode: $LiFePO_4$-composite with high volumetric capacity. *Ceram. Int.* 43(17):15370–74
62. Berbano SS, Guo J, Guo H, Lanagan MT, Randall CA. 2017. Cold sintering process of $Li_{1.5}Al_{0.5}Ge_{1.5}(PO_4)_3$ solid electrolyte. *J. Am. Ceram. Soc.* 100(5):2123–35
63. Leng H, Huang J, Nie J, Luo J. 2018. Cold sintering and ionic conductivities of $Na_{3.256}Mg_{0.128}Zr_{1.872}Si_2PO_{12}$ solid electrolytes. *J. Power Sources* 391(4):170–79
64. Funahashi S, Guo J, Guo H, Wang K, Baker AL, et al. 2017. Demonstration of the cold sintering process study for the densification and grain growth of ZnO ceramics. *J. Am. Ceram. Soc.* 100(2):546–53
65. Guo J, Guo H, Heidary DSB, Funahashi S, Randall CA. 2017. Semiconducting properties of cold sintered V_2O_5 ceramics and Co-sintered V_2O_5-PEDOT:PSS composites. *J. Eur. Ceram. Soc.* 37(4):1529–34
66. Chen WT, Gurdal AE, Tuncdemir S, Guo J, Guo H, Randall CA. 2017. Considering the possibility of bonding utilizing cold sintering for ceramic adhesives. *J. Am. Ceram. Soc.* 100(12):5421–32
67. Guo H, Bayer TJM, Guo J, Baker A, Randall CA. 2017. Current progress and perspectives of applying cold sintering process to ZrO_2-based ceramics. *Scr. Mater.* 136:141–48
68. Vaataja M, Kahari H, Juuti J, Jantunen H. 2017. Li_2MoO_4-based composite ceramics fabricated from temperature- and atmosphere-sensitive MnZn ferrite at room temperature. *J. Am. Ceram. Soc.* 100(8):3626–35
69. Liu Y, Sun Q, Wang D, Adair K, Liang J, Sun X. 2018. Development of the cold sintering process and its application in solid-state lithium batteries. *J. Power Sources* 393(3):193–203
70. Kingery WD. 1959. Densification during sintering in the presence of a liquid phase. I. Theory. *J. Appl. Phys.* 30(3):301–6
71. Kingery WD, Woulbroun JM, Charvat FR. 1959. Densification during sintering in the presence of a liquid phase. II. Experimental. *J. Appl. Phys.* 30(3):307–10
72. Kang X, Floyd R, Lowum S, Cabral M, Dickey E, Maria J-P. 2019. Mechanism studies of hydrothermal cold sintering of zinc oxide at near room temperature. *J. Am. Ceram. Soc.* In press. **https://doi.org/10.1111/jace.16340**
73. Du J, Rimsza JM. 2017. Atomistic computer simulations of water interactions and dissolution of inorganic glasses. *NPJ Mater. Degrad.* 1(1):16
74. Manzano H, Zhang W, Raju M, Dolado JS, López-Arbeloa I, Van Duin ACT. 2018. Benchmark of ReaxFF force field for subcritical and supercritical water. *J. Chem. Phys.* 148(23):234503

75. Kingery WD, Woulbroun JM, Charvat FR. 1963. Effects of applied pressure on densification during sintering in the presence of a liquid phase. *J. Am. Ceram. Soc.* 46(8):391–95
76. Coble RL. 1970. Diffusion models for hot pressing with surface energy and pressure effects as driving forces. *J. Appl. Phys.* 41(12):4798–807
77. Renard F, Bernard D, Thibault X, Boller E. 2004. Synchrotron 3D microtomography of halite aggregates during experimental pressure solution creep and evolution of the permeability. *Geophys. Res. Lett.* 31(7):L07607
78. Guo J, Pfeiffenberger N, Beese A, Rhoades AM, Gao L, et al. 2018. Cold sintering $Na_2Mo_2O_7$ ceramic with polyetherimide (PEI) polymer to realize high-performance composites and integrated multilayer circuits. *ACS Appl. Nano Mater.* 1(8):3837–44
79. Guo J, Berbano SS, Guo H, Baker AL, Lanagan MT, Randall CA. 2016. Cold sintering process of composites: bridging the processing temperature gap of ceramic and polymer materials. *Adv. Funct. Mater.* 26(39):7115–21
80. Shin YK, Sengul MY, Jonayat A, Lee W, Gomez E, et al. 2018. Development of a ReaxFF reactive force field for lithium ion conducting solid electrolyte $Li_{1+x}Al_xTi_{2-x}(PO_4)_3$ (LATP). *Phys. Chem. Chem Phys.* 20(34):22134–47
81. Clarke DR. 1987. On the equilibrium thickness of intergranular glass phases in ceramic materials. *J. Am. Ceram. Soc.* 70(1):15–22
82. Volz E, Roosen A, Wang S-C, Wei W-CJ. 2004. Formation of intergranular amorphous films during the microstructural development of liquid phase sintered silicon carbide ceramics. *J. Mater. Sci.* 39(13):4095–101
83. Cantwell PR, Tang M, Dillon SJ, Luo J, Rohrer GS, Harmer MP. 2014. Grain boundary complexions. *Acta Mater.* 62(1):1–48
84. Guo J, Zhao X, Herisson de Beauvoir T, Seo J-H, Berbano SS, et al. 2018. Recent progress in applications of the cold sintering process for ceramic-polymer composites. *Adv. Funct. Mater.* 28(39):1801724
85. Zhao X, Guo J, Wang K, Herisson de Beauvoir T, Li B, Randall CA. 2018. Introducing a ZnO-PTFE (polymer) nanocomposite varistor via the cold sintering process. *Adv. Eng. Mater.* 20:1700902
86. Zhao Y, Berbano SS, Gao L, Wang K, Guo J, et al. 2019. Cold-sintered V_2O_5-PEDOT:PSS nanocomposites for negative temperature coefficient materials. *J. Eur. Ceram. Soc.* 39(4):1257–62
87. Seo JH, Verlinde K, Guo J, Heidary DSB, Rajagopalan R, et al. 2018. Cold sintering approach to fabrication of high rate performance binderless $LiFePO_4$ cathode with high volumetric capacity. *Scr. Mater.* 146:267–71
88. Guo J, Legum B, Anasori B, Wang K, Lelyukh P, et al. 2018. Cold sintered ceramic nanocomposites of 2D MXene and zinc oxide. *Adv. Mater.* 30(32):1801846
89. Heidary DSB, Guo J, Seo JH, Guo H, Rajagopalan R, Randall CA. 2018. Microstructures and electrical properties of V_2O_5 and carbon-nanofiber composites fabricated by cold sintering process. *Jpn. J. Appl. Phys.* 57(4):025702
90. Nie J, Zhang Y, Chan JM, Huang R, Luo J. 2018. Water-assisted flash sintering: flashing ZnO at room temperature to achieve ~98% density in seconds. *Scr. Mater.* 142:79–82
91. Castro RHR, Gouvêa D. 2016. Sintering and nanostability: the thermodynamic perspective. *J. Am. Ceram. Soc.* 99(4):1105–21
92. Tikare V, Braginsky M, Olevsky EA. 2003. Numerical simulation of solid-state sintering. I. Sintering of three particles. *J. Am. Ceram. Soc.* 86(1):49–53
93. Sengul MY, Randall CA, Van Duin A. 2018. ReaxFF molecular dynamics simulation of intermolecular structure formation in acetic acid–water mixtures at elevated temperatures and pressures. *J. Chem. Phys.* 148(16):164506
94. Sengul MY, Randall CA, Van Duin A. 2018. ReaxFF molecular dynamics study on the influence of temperature on adsorption, desorption and decomposition at the acetic acid/water/ZnO($10\bar{1}0$) interface enabling cold sintering. *ACS Appl. Mater. Interfaces* 10(43):37717–24
95. Randall CA, Guo J, Baker A, Lanagan M, Guo H. 2017. *Cold sintering ceramics and composites*. US Patent Appl. 15/277,553

Annual Review of
Materials Research

Volume 49, 2019

Contents

Computational Methods in Materials

Topological Quantum Materials

Current Interest

Indexes

Errata

An online log of corrections to *Annual Review of Materials Research* articles may be found at http://www.annualreviews.org/errata/matsci